Traction Force Microscopy with DNA FluoroCubes

Armina Mortazavi[a, c], Jianfei Jiang[a, c], Philip Laric[a], Dominic A. Helmerich[b], Rick Seifert[b], Markus Sauer[b], Benedikt Sabass[a, c*]

a Department of Veterinary Sciences, Institute for Infectious Diseases and Zoonoses, Ludwig-Maximilians-Universität München, Munich 80752, Germany

b Department of Biotechnology and Biophysics, Biocenter, University of Würzburg, Am Hubland, Würzburg 97074, Germany

c Faculty of Physics and Center for NanoScience, Ludwig-Maximilians-Universität München, 80752 Munich, Germany

Abstract

From cell differentiation to morphogenesis and cell migration, a multitude of processes are coordinated by mechanical forces that cells generate. Among diverse techniques to assess the mechanical properties of the cell, traction force microscopy (TFM) has emerged as one of the most popular methods for quantifying cell-generated stresses. Standard TFM procedures rely on fiducial markers in the extracellular environment to measure the deformations that are caused by cellular forces. Typically, fluorescent beads are used as fiducials. However, the replacement of beads with fluorescently labeled DNA structures can have numerous advantages, including a smaller size of the markers and the possibility of customizing the DNA structures, for example to read out orthogonal information or to realize a switchable surface functionalization. Here, we develop a multi-purpose platform for combining such setups with TFM. As fiducials we employ FluoroCubes – nanometer-sized DNA constructs - for TFM. These constructs are grafted to a high refractive index polyethylene siloxane surface for the precise tracking of displacements resulting from cell-generated forces. To ensure a local transmission of traction forces from the adhesion ligands to the substrate, we also graft RGD peptides, which represent the smallest ligands of the extracellular matrix, onto our elastic substrates. To further enhance the spatial resolution of the TFM, FluoroCubes can be supplemented with densely packed fluorescent beads as fiducials. We propose a modification of the Kanade-Lucas-Tomasi (KLT) optical flow tracking (OFT) algorithm for optimal, simultaneous tracking of FluoroCubes and beads. Together, the developed experimental setup and tracking algorithm yield highly resolved maps of traction forces that correlate well with the spatial distribution of kindlin at focal adhesions.

Keywords: Traction force microscopy; DNA constructs; Mechanobiology; Cell adhesion

Introduction

Cell-generated forces are an integral part of many physiological and pathophysiological processes, for example, during embryogenesis, tissue development, wound healing, and immune response[1]. Traction force microscopy (TFM) is a widely-adopted method for quantifying these forces due to its versatility, robustness, and ability to capture the dynamic micromechanics of living cells as they interact with their environment[2–4]. Following the seminal work of Harris et al. in the 1980s, who demonstrated that adherent cells could induce wrinkles in thin silicone substrates, Dembo et al. were able to measure spatial maps of cell-generated traction using substrates with a linear elastic response[5,6]. In a typical TFM experiment, cells are seeded onto an elastic gel containing fluorescent beads as fiducial markers. As the cells interact with the gel substrate, they exert mechanical forces that displace the gel and, with it, the fluorescent beads. Bead displacement is monitored by optical fluorescence microscopy to assess the deformation of the gel relative to its relaxed state. The magnitude and direction of the locally exerted surface stress is then calculated by modeling the mechanical response of the substrate[7].

The accuracy of the reconstructed traction maps depends on the amount of information provided by the measurement of the cell-induced deformations. In particular, the spatial interval at which the deformations are sampled limits the resolution of traction on small length scales. To visualize traction force patterns on lengths comparable to subcellular structures, displacements must be finely sampled. As a result, several experimental methods have been developed to improve the acquired microscopy data for quantification of displacement variations on short length scales. These methods are mainly based on increasing the density of fiducial marker beads and/or using super-resolution microscopy. Examples include the combination of two types of beads with different emission spectra, the use of Stimulated Emission Depletion (STED) super-resolution microscopy, and the use of fluctuation analysis to recover high-resolution images of fluorescent beads based on spinning disk confocal microscopy[8–10]. More recently, enhanced tracer density super-resolution microscopy (ETD-srTFM) has been introduced, which improves the conjugation efficiency of the beads on the substrate and makes use of structured-illumination microscopy (SIM)-TFM. With 100 nm fluorescent beads as markers, densities of $15/\mu m^2$, corresponding to a sampling interval of 258 nm have been reported [11], which in principle allows one to resolve traction forces at a resolution of roughly 0.5 μm, according to the Nyquist theorem. Thus, a resolution of traction forces on a truly molecular scale, or even on the scale of tens of nanometers, is still far from being achieved with

conventional TFM methods that rely on the measurement of substrate deformations. In this work, we investigate how the use of DNA-origami-based FluoroCubes as fiducial markers, together with other experimental modifications, can provide an avenue for improving the resolution and versatility of classical TFM methods.

To provide context, we begin with a brief introduction to the procedures typically used to calculate cellular tractions from microscopy data with a standard setup. The calculation of cellular tractions is based on pairs of microscopy images containing fiducial makers, such as fluorescent beads, to visualize the substrate deformations in the vicinity of cells with respect to images of the undeformed substrate without cells, which are typically removed by trypsinization. After the acquisition of high-resolution images of the cell and the fiducial makers, the next step is to quantify the deformations of the substrate. For this purpose, the displacement of fiducials between image pairs is determined using either Particle Tracking Velocimetry (PTV) or Particle Image Velocimetry (PIV). In PTV, the motion of individual fiducial markers is tracked to generate dense displacement fields[12]. However, an accurate localization and assignment of fiducials in the image pairs is necessary for single-particle tracking, which can be challenging for dense fluorescent probes with overlapping point spread functions (PSFs). In contrast, PIV can robustly quantify displacements in an image that is divided into small windows that can contain more than one fiducial. The displacement of each window in one image with respect to another image is obtained by maximizing its cross-correlation with respect to a local, relative shift of the images[13]. Besides PIV and PTV, Optical Flow Tracking (OFT) has recently emerged as a method to quantify the displacements in a TFM experiment with high precision and spatial resolution[14]. Similar to PIV, OFT relies on local image features and does not require precise localization of the individual particles. Object tracking requires interrogation windows and, within each window, OFT requires intensity consistency[15] and local smoothness[16]. If these conditions are met, dense clusters of fiducial markers can be tracked even if their PSFs overlap strongly[17,18]. However, analogous to PIV, the size of the window affects the smoothness of the resulting displacement field in OFT. Large window sizes result in smooth displacement fields that contain little noise, while small window sizes can capture local details of the displacement field at the cost of being more susceptible to noise. Once a displacement field has been extracted from the data, the spatial map of cell-generated tractions can be computed using various methods. The most widely used methods are based on Green's functions that relate a displacement field to the application of a point-like surface traction[6,19]. Among these methods, Fourier Transformation Traction Cytometry (FTTC) stands out due to its robustness and computational efficiency[8,20]. Calculation of the traction

fields in the Fourier domain drastically reduces the required computational effort. Detrimental noise in the displacement field can be dealt with by classical regularization schemes or by Bayesian Fourier Transformation Traction Cytometry (BFTTC) [21].

In this work, we aim to replace fluorescent marker beads with molecular-sized probes as fiducial markers for TFM. The DNA-based FluoroCubes introduced in Ref.[22] are approximately 6 nm in size and comprise multiple fluorophores to improve overall photostability. Substrates can be labeled with densely spaced FluoroCubes and these probes can in principle be used for super-resolution imaging with Stochastic Optical Reconstruction Microscopy (STORM). However, due to the low brightness of FluoroCubes, their use in a TFM experiment requires the development of dedicated cell substrates and analysis software. Here, we attach the FluoroCubes to the surface of high refractive-index silicone substrates, which allows us to improve image quality by using total internal reflection fluorescence (TIRF) microscopy[23–25]. Although this setup did not allow reliable displacement tracking in combination with STORM, regular TIRF images of FluoroCubes can be used for tracking at high resolution. In addition to FluoroCubes, fluorescent nanobeads with a complementary emission spectrum can be conjugated to the substrates. For tracking substrate displacements that occur simultaneously in two microscope channels, we propose a custom modification of the classical Kanada-Lucas-Tomasi OTF algorithm[15,18]. The developed methods are validated using synthetic and experimental data.

Results

In the following, we present results from the development of FluoroCube-based TFM methods, including experimental procedures and image analysis.

Substitution of PAA substrates with PDMS substrates improves image quality

Established materials for cell substrates in TFM experiments are either hydrogels or elastomers, such as polyacrylamide (PAA) or polydimethylsiloxane (PDMS), respectively, which allow for a tunable stiffness roughly between 100 Pa and 50 kPa. Since hydrogels and elastomers have quite different optical properties, we systematically compare these substrates to achieve an optimal image quality before switching to fluorescent fiducial markers that are much less bright than the standard beads. For PAA hydrogels used in a standard TFM approach, the fluorescent beads are typically incorporated into the gels by mixing them with the gel constituents prior to polymerization. However, the presence of the beads throughout the gel causes light scattering, diffraction, and results in a large background fluorescence if the fluorophores are excited

outside of the focal plane (Fig. 1a). Additionally, the different axial positions result in distorted or obscured images of the beads in a wide-field image. Mixing the beads with the PAA gel components can also result in clusters of beads, which appear as bright spots under the microscope and thus prevent the tracking of individual beads. Potentially, the clusters can even lead to unwanted spatial variations in the material parameters that govern the mechanical response of the gel. Overall, the embedding of fiducial markers inside of the gels makes the accurate data analysis and the interpretation of traction force maps a challenging task. However, fluorescent beads can also be attached only to the gel surfaces, which improves control over their spatial distribution in the image plane and improves data quality[26], see Fig. 1b. As hydrogels, PAA substrates have the potential drawback of exhibiting quite large pore sizes in the range of [10-40] nm, depending on the typically used concentrations of gel constituents[27]. This pore size implies that the surface topography is likely inhomogeneous on length scales comparable to the size of the subcellular structures that transmit the traction force, which can be an issue for truly molecular-scale traction resolution. Moreover, the stiffness of PAA substrates can be affected by the composition of the imaging buffer and will change over time as the gel swells[28,29]. Finally, the transparency of PAA gels may decrease with increasing crosslinking density.

PDMS substrates provide certain advantages over PAA gels due to their excellent optical transparency, allowing for efficient excitation and detection of fluorophores, see Fig. 1c. Furthermore, the use of high-refractive-index PDMS substrate makes it possible to image fluorescent molecules close to the surface in a total internal reflection fluorescence (TIRF) – like mode (“dirty TIRF”)[24,25]. For PDMS substrates made with the Dow DOWSIL™ CY 52-276 Kit, we find that TIRF microscopy further enhances the signal-to-noise ratio, see Fig. 1d.

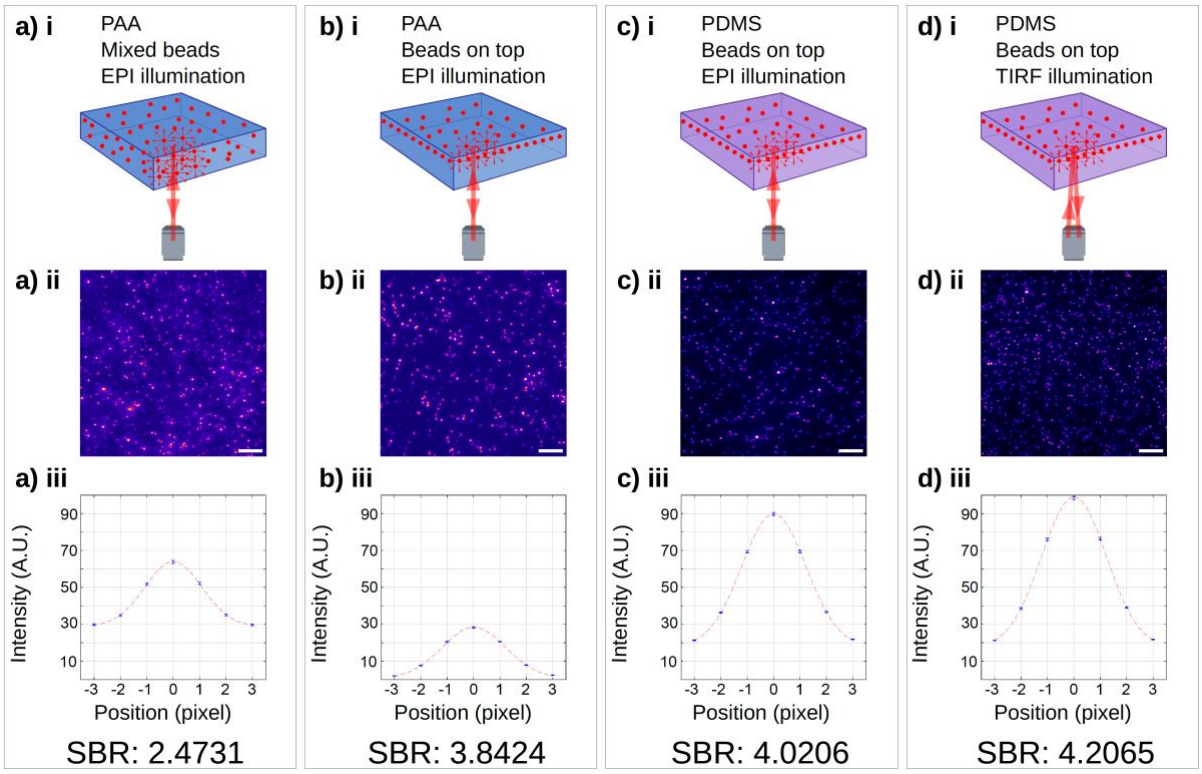

Fig. 1. Comparison of image quality achieved with different gel substrates for TFM. All substrates have an approximate thickness of 100 nm. a) 40 nm, red-orange fluorescent carboxylate-modified microspheres are mixed with PAA gel solution (0.31 beads·μm^{-2}) and imaged in EPI illumination mode, b) Beads are conjugated to the top surface of a PAA gel (0.25 beads·μm^{-2}) and imaged with EPI illumination mode. c) Beads are conjugated to the top surface of a PDMS (0.25 beads·μm^{-2}) gel and imaged with EPI illumination mode, d) Beads are conjugated to the top of a PDMS gel (0.29 beads·μm^{-2}) and imaged in TIRF illumination mode. i) Illustrations of the different setups. ii) Images of beads, scale bars: 5 μm. iii) Fluorescence intensity profiles around beads as an estimate for the point-spread function. Data is averaged over all detected beads in the images. Red dashed lines are fitted Gaussian functions, blue dots are average intensities along the central horizontal line of the individual bead image with error bars indicating the standard error of the mean. SBR: signal to background ratio. Comparison of the data in (a-d) shows that PDMS substrates result in better image contrast, fewer out-of-focus signals, and a lower background, which improves separation of signals from neighboring beads.

Dual labeling of substrates with FluoroCubes and beads

Use of FluoroCubes, which have a size similar to the green fluorescent protein, allows one to increase the density of markers on the substrate, improving the spatial coverage of the traction force maps. However, a FluoroCube with 6 fluorescent dyes emits fewer photons than a

fluorescent bead with 100s of dyes, making it harder to precisely localize. To increase localization precision, we label the PDMS substrates with beads in addition to fluorescent probes of varying sizes and colors. Fig. 2a illustrates the structure of the dual-labeled surface coating. Briefly, the hydrophilicity of the PDMS surfaces is improved through functionalization with amine groups, followed by passivation with biotinylated bovine serum albumin (BSA). This process allows for the conjugation of neutravidin to the substrate, which, in turn, enables high-affinity binding of FluoroCubes with biotin moieties. RGD peptides, as a substitute for larger extracellular matrix proteins, and carboxylate-modified microspheres are then activated with carbodiimide and reacted with amine groups of the substrate to form amide bond derivatives, see Fig. 2b[30,31]. Functionalized PDMS substrates can be imaged in TIRF mode. Given the observed blinking behavior of FluoroCubes, we employed direct stochastic optical reconstruction microscopy (*d*STORM) to precisely localize and track individual FluoroCubes[32]. However, we found that super-resolution tracking of fluorophores was only possible for sparsely distributed probes and therefore *d*STORM provided little advantage over diffraction-limited imaging with regard to traction-force resolution. Various biocompatible STORM buffers were tested but did not improve blinking behavior of the Cy5 dye molecules associated with FluoroCubes sufficiently, see Supplementary Information. In addition, the high-intensity laser and long acquisition time of *d*STORM could affect the cells' morphology, which in turn changes the traction patterns[33]. However, regular TIRF images of FluoroCubes can be acquired at low laser power and allow one to track the surface displacements.

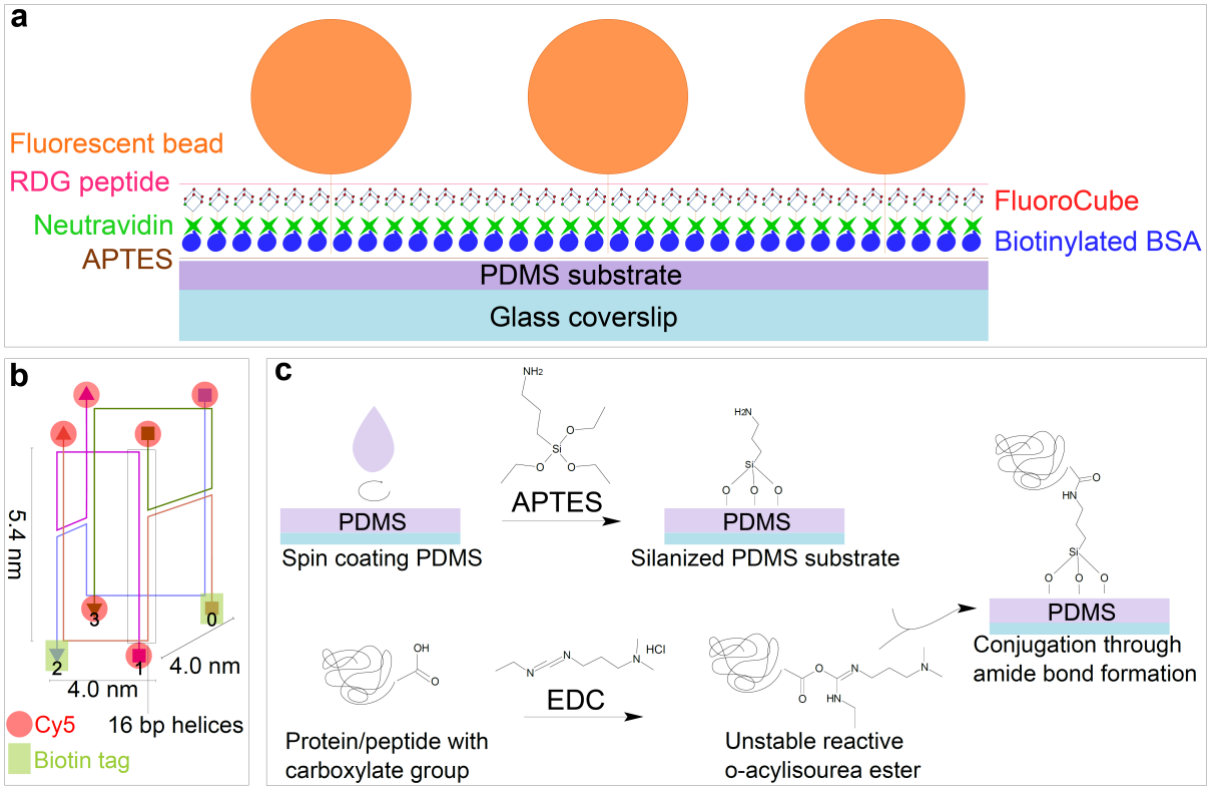

Fig. 2. Functionalization of silicone substrates for traction force microscopy with FluoroCubes. a) PDMS substrates are passivated with biotinylated bovine serum albumin (BSA) after functionalization with aminosilane (3-Aminopropyl)triethoxysilane (APTES). As a linker molecule, streptavidin reported in Ref.[22] was replaced with neutravidin, which forms a complex with FluoroCubes attached to a biotin tag at one site and biotinylated BSA at another site. 40 nm carboxylated beads are bound to the substrate and the substrate is subsequently functionalized with RGD peptides for cell adhesion. b) FluoroCubes comprise six Cy5 dyes and two biotin molecules, all conjugated to 32 bp ssDNA that is folded subsequently. c) Conjugation of beads and peptides starts with activation of carboxylate by 1-ethyl-3-(3-dimethylaminopropyl) carbodiimide (EDC). EDC-mediated conjugation leads to formation of a highly reactive *O*-acylisourea intermediate that forms an amide bond with amine groups on the surface of the PDMS substrate.

Modified optical flow tracking for improved traction-force resolution with dual-labeled samples

For inference of a displacement field, we compare images of beads and FluoroCubes in presence of a cell with images of the same region after removal of the cell by trypsinization. A versatile Kanada-Lucas-Tomasi (KLT) optical flow tracking algorithm is used to analyze the images (see methods). However, the standard KLT algorithm can only track displacements from pairs of images recorded in one fluorescence channel, e.g. only from images of the beads. Therefore, we perform tests with synthetic data to find out how to optimally extract coherent deformation fields from pairs of images recorded in the two channels corresponding to FluoroCubes and beads. The synthetic data consists of a high-resolution displacement fields (Fig. 3ai) and traction fields (Fig. 3aii) where tractions are to be reconstructed based on an area density of markers of around 5 μm^{-2} to replicate the images obtained from our experimental setup. We analyze the displacement fields generated with different OFT schemes and also compare the corresponding traction fields as illustrated in Fig. 3. Note that one could also employ post-processing methods to exclude tracking errors from the final data. This, however, is not done here since we are interested in evaluating the performance of the algorithmic modifications of OFT.

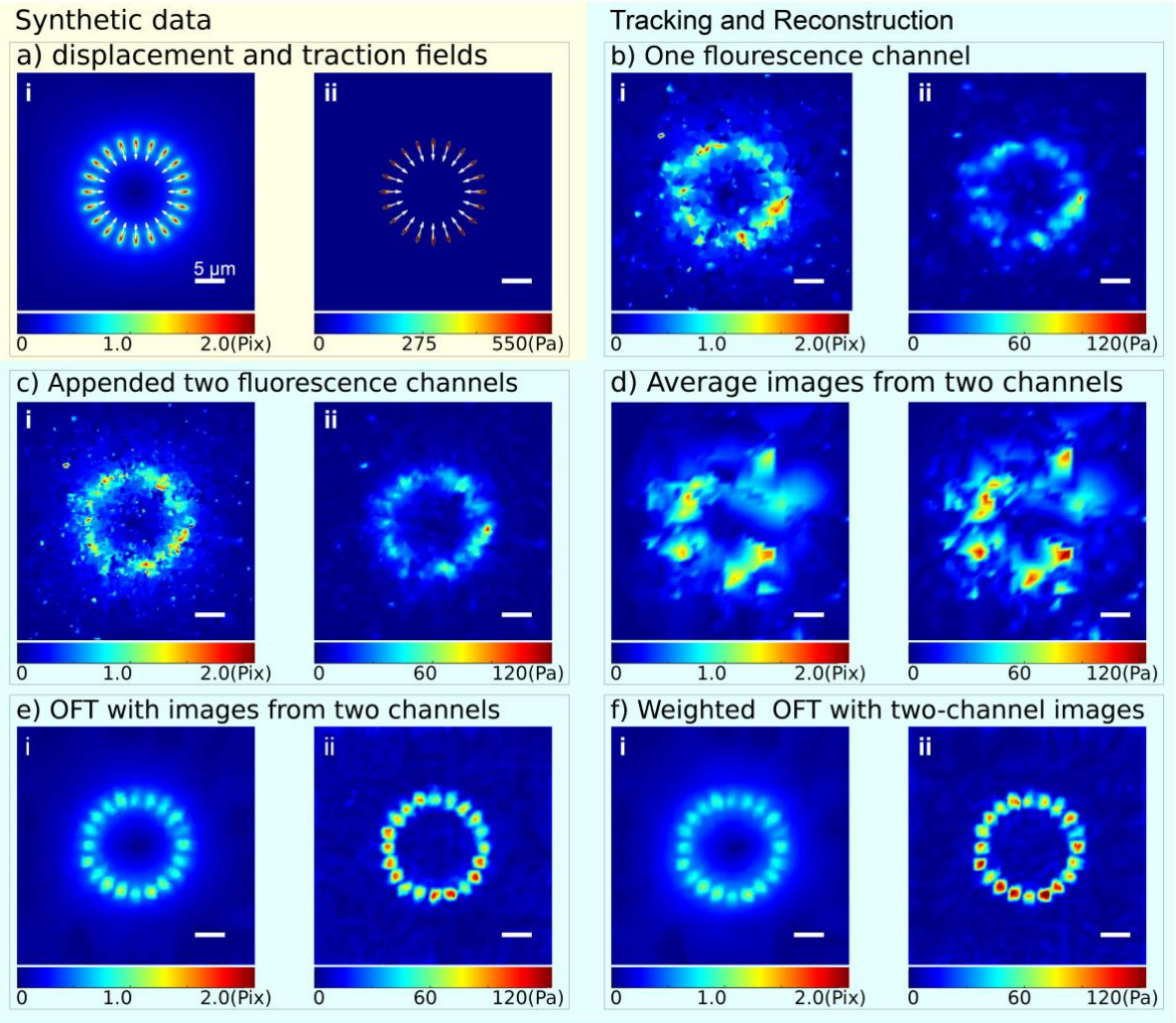

Fig. 3. Optimization of TFM resolution by combining information from two fluorescence channels requires a modified KLT tracking algorithm. The two channels correspond to images of FluoroCubes and beads, respectively. a) Synthetic displacement field (i) generated from a pre-defined traction pattern (ii); b) Displacement field resulting from OFT in only one of the two channels (i) and the traction field reconstructed from this data (ii); c) Displacements resulting from independent OFT in both channels and subsequent appending of both data sets (i) and tractions reconstructed from this data (ii). Note the large noise resulting from independent tracking of both channels; d) Displacements resulting from OFT in images that were created by superposition of the fluorescence signals from both channels (i) and reconstructed tractions (ii). Averaging fluorescence signals in the images degrades traction resolution since trackable features in individual images are covered and distorted; e) Displacement field extracted from both channels with modified KLT tracking routine (i) and resulting traction field (ii). Concatenation of the two datasets in the linear equations used for KLT improves tracking; f) Displacements extracted from both channels using a modified KLT

tracking routine with cross-correlation-based weighting factors (i) and its corresponding traction field (ii). Color bars indicate the magnitudes of displacement and traction fields. Scale bar: 5 µm.

Use of either of the two channels, representing either FluoroCubes or beads, allows one to reconstruct traction forces at rather low resolution where individual spots of traction are not clearly discernible, see Fig. 3b. As a first attempt to combine information from both pairs of images, we track the displacements in both channels independently and append the results, which in principle provides a denser field. However, this approach hardly improves the spatial resolution of traction forces since tracking errors in the two independent channels result in strong local misalignment and magnitude mismatch of the displacements from the two channels, see Fig. 3c. Similarly, averaging the images from two fluorescence channels does not improve the resolution because meaningless cross-channel correlations appear in the objective function and because image superposition smooths out intensity variations that are required for tracking, see Fig. 3d. However, an extension of the optical flow tracking algorithm to optimize coherent motion in both channels can eliminate this issue, resulting in reliable displacement and traction fields with high resolution, see Fig. 3e. Furthermore, a cross-correlation-based weighting scheme can be applied to take into account different levels of uncertainty in the two sets of data, which further enhances the reliability and resolution of the traction force fields, see Fig. 3f. Due to the low noise level in the data, reconstruction of traction forces from displacements that are extracted with the modified OTF algorithms requires little additional smoothing (small regularization) (Supplementary Table 1).

Comparison of the resulting estimated displacement vectors with the ground truth reveals a consistent underestimation of the magnitude. This underestimation is also common for PIV-based methods and can be attributed here to the smoothness assumptions intrinsic to the KLT optical flow method. Consequently, the reconstructed traction fields are underestimated, as is the case for other methods[8,20,21].

High-resolution TFM on substrates labeled with FluoroCubes and beads

We next demonstrate that the modified setup allows high-resolution TFM experiments. For experiments with cells, coverslips are spin-coated with high refractive-index PDMS elastomer and the sample is subsequently affixed to sticky chambers containing 8 or 18 wells. Inspired by methods proposed in Ref.[34], this setup enables an efficient preparation of samples replicates

that can be imaged separately or during one session. The densities of both types of fluorescent probes is adjusted carefully to be as high as possible, while still allowing the distinction of individual fiducial markers with a diffraction-limited microscope for subsequent motion tracking. The resulting number densities are ~4 and ~7 per square micrometer depending on the image acquisition and reconstruction technique (Supplementary Fig. 1). This density determines the spatial resolution of traction forces. Note that some previous work on the use of super-resolution microscopy for TFM relies on a much lower label density[9,10] or on PIV with relatively large correlation windows[35], which makes it challenging to reconstruct traction maps with sub-micrometer resolution. To reduce noise resulting from blinking fluorophores, images in this experiment are generated by averaging 100 rapidly acquired frames for FluoroCubes and 50 frames for the beads. To assess the reliability of FluoroCube tracking, we first compare the results from tracking only the FluoroCubes with the corresponding results from the analysis of bead images. Measured displacement fields and reconstructed traction fields of FluoroCubes and beads are qualitatively in agreement with each other, see Fig. 4(b-c). Due FluoroCube blinking and low signal-to-noise ratio, the displacement field extracted from FluoroCubes contains some noise and spurious traction spots outside the area covered by the cell, see Fig. 4c-ii. Using our modified OFT algorithm for simultaneous analysis of both channels, the contributions of the noisy channel are suppressed in the optical flow calculation, resulting in a smooth high-resolution TFM result, see Fig. 4d. The quality of the traction field can be gauged by visual inspection of the co-localization of traction forces with fluorescence intensity of labeled focal-adhesion proteins. We employ cells that stably express fluorescent Kindlin-2 ($Kind^{Ko+K2GFP}$). Kindlins are core focal-adhesion proteins that, together with talin, bind the β-integrin cytoplasmic tails and also links the integrin tails to the contractile F-actin cytoskeleton[36,37].Therefor, we expect that traction forces transmitted by integrins occur in close proximity to accumulations of kindlin. Fig. 4b-d illustrate that while the traction forces calculated from the data in the two individual channels are indeed located in proximity of focal adhesion sites, the combination of both channels reveals more details of the traction fields as a consequence of the higher number of trackable data points.

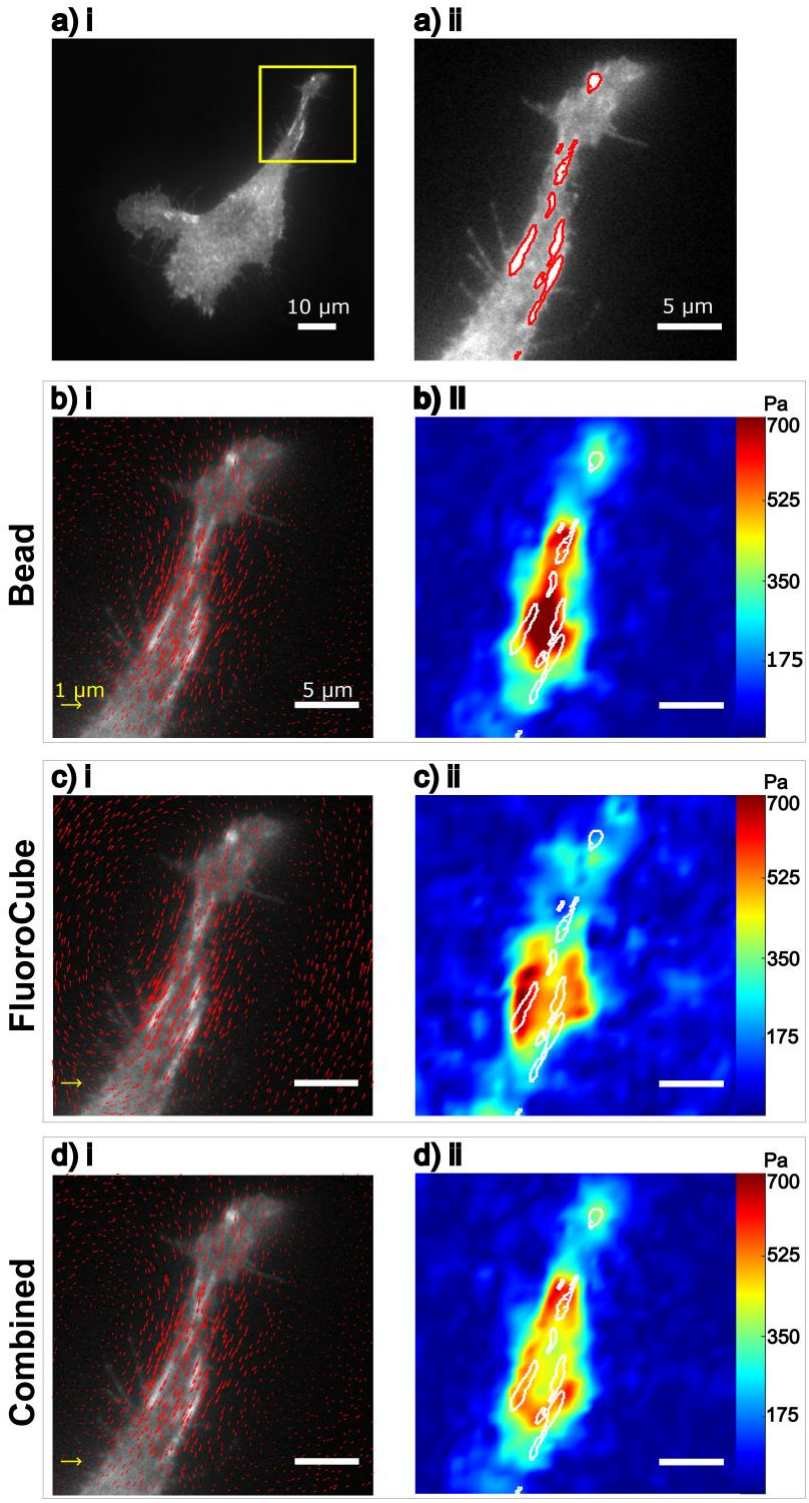

Fig. 4. Demonstration of TFM with FluoroCubes and fluorescent beads as fiducial markers. a) Image of a murine kidney fibroblast with GFP-labeled kindlin-2 ($Kind^{Ko+K2GFP}$ cell line); b)-(i) Displacements of the PDMS substrate calculated only from tracking beads; b)-(ii) Tractions calculated from the data in (i) with BFTTC; c)-(i) Displacements calculated only from tracking FluoroCubes; c)-(ii) Tractions calculated from FluoroCube tracking data d)-(i) Displacements calculated with weighted, 2-channel KLT tracking algorithm; d)-(ii) Corresponding tractions co-localize with fluorescently labeled kindlin-2 at focal adhesions.

Concluding discussion

Classical TFM methods based on the measurement of substrate deformation are well established and readily available in many laboratories. They can be performed with basic equipment and are quite versatile[38]. A wide range of sample sizes can be studied, from very small cells to large multicellular systems[39]. Sophisticated analysis methods make it possible to study cellular forces in three-dimensional geometries or on complex topographies[7], as well as in the presence of external perturbations[55]. Other advantages of classical TFM are that the method produces vectorial traction results and is able to detect force magnitudes in a very wide range, starting from a few pN measured for bacterial appendages on soft substrates to forces of up to 600 nN for platelet adhesions that are important for blood clot formation[40–42]. Finally, conventional TFM setups can be used for studying cells with relatively high throughput. This is facilitated by the utilization of microfabrication methods to generate regular patterns of fiducial markers, so that substrate deformations can be quantified without having to record an undeformed reference state[43,44].

A potential drawback of classical TFM is its limited spatial resolution. A typical resolution limit in the range of a few μm can be a problem when traction force patterns need to be characterized in fine detail, e.g. to study the function of subcellular structures or to measure the forces generated by small bacteria. More recently developed techniques to measure cellular forces with high spatial resolution, albeit in a limited force range, rely on molecular force sensors that are directly linked to the adhesion molecule ligands and are grafted onto a rigid surface onto which cells are seeded[45–49]. Recently, such sensors have even been combined with soft hydrogel substrates[50]. DNA-based sensor molecules attached to a substrate can also allow local readout of various other cellular signals[51]. For example, to quantify the local release of dopamine by cells[52]. Finally, coating surfaces with engineered ligands also allows local control of cell adhesion, e.g. with RGD-functionalized azobenzenes[53,54].

In this work, we aim to refine the experimental setup and image analysis procedures to combine the advantages of classical TFM with substrate functionalization by DNA-based constructs. The replacement of marker beads incorporated into PAA gels by FluoroCubes attached to silicone substrates with negligible pore sizes, in principle has the potential to yield molecular-scale traction resolution on the order of tens of nanometers. However, we encountered limitations in utilizing *d*STORM for effective substrate deformation analysis. This was primarily due to challenges in reliably tracking dense, super-resolved labels. Moreover, the detrimental effects

of high laser intensities and prolonged acquisition times on living cells further hindered our ability to conduct the analysis successfully. Instead, FluoroCubes, with their exceptional photostability, proved suitable for motion tracking in regular brightfield images. This data can be combined with data obtained by tracking fluorescent beads to provide high-resolution traction data. Exemplary results obtained with this technique showed that kindlin-2 is highly colocalized with the magnitude of traction at focal adhesions. The proposed methods are intended to serve as a basis for the development of advanced setups that combine TFM with local measurement of cellular signals on a surface.

Author contributions

AM and PL performed experiments; JJ wrote the code. AM, JJ and BS analyzed the data; DAH, RS, and MS provided fluorescent constructs. All authors participated in the writing of the manuscript.

Acknowledgments

The authors gratefully acknowledge the generous gift of $Kind^{Ko+K2GFP}$ cells from Prof. Dr. Reinhard Fässler (MPI of Biochemistry, Munich, Germany) and the gift of constructs and cell lines from Prof. Dr. Carsten Grashoff (University of Münster, Germany). AM, JJ and BS received funding from the European Research Council (ERC) under the European Union's Horizon 2020 research and innovation programme (BacForce, G.A.No. 852585). JJ and BS acknowledge funding by the Deutsche Forschungsgemeinschaft (DFG, German Research Foundation), Project no 492014049. DAH, RS and MS received funding from ERC under the European Union's Horizon 2020 research and innovation funding programme (G.A.No. 835102).

Materials and Methods

Cell Culture

Human foreskin fibroblasts (ATCC; SCRC-1041) and $Kind^{Ko+K2GFP}$ cells ($Kind^{Ko}$ immortalized murin kidney fibroblast reconstituted with green fluorescent protein-tagged kindlin-2 expression plasmids, generous gift from Prof. Dr. Reinhard Fässler, PMID: 26821125) were cultured at 37 °C and 5% CO_2 in Dulbecco's modified Eagle's medium

(DMEM; Sigma-Aldrich, D6546), supplemented with 10% fetal bovine serum (FBS, Sigma-Aldrich, F2442), 4 mM L-Glutamate (Sigma-Aldrich, G7513), and 20 µg/mL gentamicin (Sigma-Aldrich, G1397). Cells were split every 2 days at a volume ratio of 1:5.

Folding and purification of FluoroCubes

A modified protocol of Ref.[22] was employed to prepare the DNA FluoroCubes. In summary, the four 32 bp oligonucleotide strands (Integrated DNA Technologies, IDT) were dissolved in deionized water to a final concentration of 100 µM. Each strand was modified with biotin, Cy5 or both, with the sequence available in the supplementary data (Supplementary Table 2). For a 50 µl folding reaction of the desired six-dye FluoroCubes, 5 µl of each of the four oligos were added to a PCR tube to reach the final concentration of 10 µM, filled with 25 µl of deionized water, and 5 µl of the 10x folding buffer (50 mM Tris pH 8.5, 10 mM EDTA and 400 mM $MgCl_2$). The samples were placed in a thermocycler to fold the six dye FluoroCubes with the following temperature ramp: Denaturation occurred at 85 °C for 5 min, followed by cooling from 80 °C to 65 °C with a decrease of 1 °C per 5 min; Further cooling was occurred from 65 °C to 25 °C with a decrease of 1 °C per 20 min; The final holding temperature was at 4 °C. Folded products were analyzed by 2.0% agarose gel electrophoresis in TBE buffer (45 mM Tris-borate and 1 mM EDTA) with 12 mM $MgCl_2$ at 70 V for 3 hours. To prevent potential unfolding, the gel box was placed in an ice bath during analysis. After completion of the gel run, it was analyzed using a custom-built system consisting of a 625 nm LED (ThorLabs, M625L3) and a bandpass filter (ET700/75, Chroma). DNA staining dyes such as ethidium bromide are prohibited to use as it will bind to the DNA and therefore might interfere with the absorbance and emission pattern of the FluoroCubes in downstream imaging applications. The desired band was then extracted from the gel using a razor blade. Afterwards, the excised band was placed in a Freeze 'N Squeeze™ DNA Gel Extraction Spin Column (BioRad, 732-6165) and centrifuged for 3 min at 12,000 rcf at 4 °C. The flow-through contained the desired FluoroCubes and were stored at 4 °C for a couple of weeks.

PDMS gel substrate preparation for traction force microscopy

Employed glass coverslips (Marienfeld, 60 × 24 mm, #1.5H) underwent a thorough cleaning process in three steps. Initially, they were sonicated in a 5% v/v solution of Hellmanex III for

10 minutes, followed by sonication in 1 M potassium hydroxide for 10 minutes and, lastly, in 100% Ethanol. During each step, the coverslips received a rigorous washing in double distilled water for 5 minutes. Finally, compressed nitrogen was used to dry the coverslips.

Silicone substrates were fabricated by combining a 1:1 or 1.2:1 weight ratio of two components Cy-A and Cy-B (Dow DOWSIL™ CY 52-276 Kit), resulting in a substrate stiffness of approximately 10 or 3 kPa, respectively. The gel solution was mixed thoroughly, centrifuged, and degassed before pipetting 100 µl of it onto a glass coverslip. The solution was spin-coated for 90 seconds using s home-made spinner, with acceleration and deceleration occurring every 30 seconds, to create a smooth, uniform surface. The gels were cured at 80 °C for 3 hours, after which they were stored at RT. To functionalize the silicone surface, the gels were treated with a solution of 7% (vol/vol) 3-aminopropyl trimethoxysilane (APTES) in pure ethanol for 2 hours. The gels were washed with pure ethanol, a 1:1 volume ratio of ethanol and PBS, and finally with PBS alone, each for three cycles.

As a cell culture and imaging chamber, an 8 well bottomless sticky-slide (Ibidi, 80828) was mounted on top of each PDMS substrate. After washing the chambers three times with PBS (Sigma-Aldrich, D8537), the surfaces were incubated with 0.5 g/L BSA-Biotin (ThermoFisher, 29130) in PBS for 2 hours at RT. Subsequently, the chambers were washed three times with PBS before incubation with 0.5 g/L Neutravidin (ThermoFisher, 31050) in PBS for 30 min at RT. The surfaces were washed three times with PBS and incubated with purified FluoroCube-DNA solution, diluted to 1 nM in PBS, for 10 min at RT. Afterwards, the prepared samples were washed at least three times in PBS.

A solution of 40 nm, red-orange fluorescent (565/580) FluoSpheres carboxylate-modified microspheres (Invitrogen, F8794) at a dilution of 1:1,000 in PBS was mixed with a final concentration of 100 µg/mL EDC and pipetted onto the top surface of the gel. The solution was incubated for 20 min at RT and washed three times with PBS. Next, the gels were coated with a solution of 10 µg/mL RGD peptides with 100 µg/mL of EDC in PBS, and incubated for 2 hours at RT or overnight at 4 °C. After incubating, the chambers underwent multiple washes, initially with PBS and then with the cell culture medium, before being seeded with cells.

PAA gel preparation

To prepare PAA gels, we used a modified protocols of Refs.[10,26]. Briefly, glass bottom dishes (35 mm dish with 14 mm bottom well #1.5, Cellvis) were activated for 5 min with a solution of 3-(Trimethoxysilyl)propyl methacrylate (Sigma-Aldrich, 440159, diluted in absolute ethanol to the final concentration of 5%) and mixed with a final concentration of 3% diluted glacial acetic

acid (diluted in water to the final concentration of 10%) to covalently link the polyacrylamide gels to the glass plates. The dishes were washed twice with ethanol and twice with distilled water and dried thoroughly before use. For the gels with fluorescent beads only on top, clean glass cover slips (#1.0 round, Ø: 12 mm) were coated with 0.1 mg/mL Poly-D-Lysine (gibco, A38904-01) for 1 hour. Aftewards, the solution was aspirated, and the cover slips were blow dried. A solution of 1:10,000 fluorescent beads diluted in PBS was prepared, vortexed and placed in ultrasonic bath for 20 min. Next, 150 µl of the solution was pipetted onto coated cover slips, then left to sit for 10 minutes before being aspirated.
For a PAA gel with a Young's modulus of 10 kPa, the following components were mixed: 1 mL of 40% bisacrylamide (BioRad, 161040), 325 µl of 2% acrylamide (BioRad, 610142), 5 µL of acrylic acid (Sigma-Aldrich, 147230), 2.5 µl Tetramethylethylenediamine (TEMED, Sigma-Aldrich, T9281), and 3547.5 µl of PBS. Immediately before pipetting the solution onto the dishes, 25 µl of 10% ammonium persulfate (APS, Sigma-Aldrich, A3678) was added. 15 µl of the gel solution was pipetted into the center of glass bottom dishes and immediately was sandwiched with a functionalized cover slip. The dishes were flipped over to ensure the fluorescent beads remained only on top. After 40 min, the dishes were flipped back and filled with PBS to facilitate the detachment of the cover slip from the gel. For the PAA gels containing fluorescent beads inside of the gel, the beads were mixed thoroughly with the gel components prior to the addition of TEMED and APS. The beads were diluted with the gel components empirically until the resulting image displayed a comparable number of detected beads as the gels with beads placed on the top.

Microscopy

All microscopy data were acquired using an inverted IX83 microscope (Olympus, Japan) with TIRF functionality, an Abbelight SAFe 360 nanoscopy module, Oxxius lasers (LPX-640-500-CSB, Oxxius, France), and using the NEO software (Abbelight, France).

To excite Cy5-FluoroCubes, 40 nm beads, and GFP-labeled proteins, the 640, 532, and 488 nm laser lines were integrated into the microscope through the ASTER technology with TIRF illumination mode. The illuminated lights were reflected onto the objective (100x oil-immersion objective, NA 1.5) with a quad-band dichroic mirror (Di03-R405/488/532/635-t1-25×36, Semrock, USA). The emitted light was initially filtered through a quadband bandpass filter (FF01-446/510/581/703-25 BrightLine quad-band bandpass filter, Semrock, USA) and subsequently with single bandpass filter (F-445/45, F-510/20. F-582/64 Semrock, USA), which

were mounted on an Optospin fast filter wheel (Cairn, England). The fluorophore emissions were recorded with a 2048 × 2048-pixel sCMOS camera (Orca-fusion C1440-20UP, Hamamatsu, Japan) with an optical pixel size of 97 nm. Before imaging, the cells were washed twice with DMEM media and then switched to the imaging buffer, which includes DMEM media with the final concentration of 0.56 mg/mL of glucose oxidase (Aspergillus niger-Type VII, lyophilized powder, Sigma-Aldrich, G2133) and 34 μg/mL of catalase (bovine liver -lyophilized powder, Sigma-Aldrich, C40). Image acquisition of FluoroCubes and fluorescent beads were performed at 50-ms intervals over 100 frames and 50 frames, respectively. After the cells were detached using 0.5% Trypsin-EDTA (Gibco, 15400054), the imaging media was exchanged to capture the gel's relaxed state.

Quantifying substrate displacements

Displacement fields are acquired by comparing images of different fiducial markers before and after detachment of the cells by trypsinization. We employ the original Kanade-Lucas-Tomasi (KLT) optical flow feature tracking algorithm[15,18] for tracking the displacements locally. The original algorithm, however, can only track motion in one fluorescence image channel. We therefore extend the KLT optical flow tracker to follow coherent motion in images recorded in two separate fluorescence channels.

Optical flow tracking

For use of the standard KLT algorithm, one considers a pair of images at two time point denoted by t and t+1. The whole image is partitioned into small interrogation windows, each containing n pixels. Finding the motion of each individual interrogation window is formulated as an optimization problem. The pixel intensities $I(\mathbf{x}_i, t)$ at positions $\mathbf{x}_i$ are is compared to pixel intensities $I(\mathbf{x}_i + \mathbf{u}, t + 1)$, where all positions in the interrogation window are shifted by the same displacement vector $\mathbf{u}$ as

$$\arg\min_{\mathbf{u}} \sum_{i=1}^{n} (\|I(\mathbf{x}_i + \mathbf{u}, t + 1) - I(\mathbf{x}_i, t)\|^2). \quad (1)$$

An expansion $I(\mathbf{x}_i + \mathbf{u}, t+1)$ is based on the assumption of small displacements $\mathbf{u}$ and yields in first order the optical flow equations, which are given by

$$\underbrace{\begin{pmatrix} I_x(x_1,y_1) & I_y(x_1,y_1) \\ \cdots & \\ I_x(x_n,y_n) & I_y(x_n,y_n) \end{pmatrix}}_{\boldsymbol{A}} \begin{pmatrix} u_x \\ u_y \end{pmatrix} + \underbrace{\begin{pmatrix} I_t(x_1,y_1) \\ \cdots \\ I_t(x_n,y_n) \end{pmatrix}}_{-\mathbf{b}} = 0, \tag{2}$$

where $I_{\mathrm{x}}(x_i,y_i) = \frac{\partial I(\mathbf{x}_i,t)}{\partial x}$, $I_{\mathrm{y}}(x_i,y_i) = \frac{\partial I(\mathbf{x}_i,t)}{\partial y}$, $I_{\mathrm{t}} = I(\mathbf{x}_i, t+1) - I(\mathbf{x}_i, t)$. This linear system is typically overdetermined since the number of pixels n is greater than the number of unknowns. Therefore, Eq. (2) can be solved with a least-square approach as

$$(\boldsymbol{A}^{\mathrm{T}}\boldsymbol{A})\mathbf{u} - \boldsymbol{A}^{\mathrm{T}}\mathbf{b} = 0, \tag{3}$$

$$\mathbf{u} = (\boldsymbol{A}^{T}\boldsymbol{A})^{-1}\boldsymbol{A}^{\mathrm{T}}\mathbf{b}, \tag{4}$$

where

$$\boldsymbol{A}^{\mathrm{T}}\boldsymbol{A} = \begin{pmatrix} \sum_{i=1}^{n}\left(I_x(x_i,y_i)\right)^2 & \sum_{i=1}^{n}\left(I_x(x_i,y_i)I_y(x_i,y_i)\right) \\ \sum_{i=1}^{n}\left(I_x(x_i,y_i)I_y(x_i,y_i)\right) & \sum_{i=1}^{n}\left(I_x(x_i,y_i)\right)^2 \end{pmatrix}, \tag{5}$$

$$\boldsymbol{A}^{\mathrm{T}}\mathbf{b} = \begin{pmatrix} \sum_{i=1}^{n}\left(I_x(x_i,y_i)I_t(x_i,y_i)\right) \\ \sum_{i=1}^{n}\left(I_x(x_i,y_i)I_t(x_i,y_i)\right) \end{pmatrix}. \tag{6}$$

Equation (3) has a well-defined solution given by Eq. (4) if $\boldsymbol{A}^{\mathrm{T}}\boldsymbol{A}$ is invertible, which requires $\mathrm{Tr}(\boldsymbol{A}^{\mathrm{T}}\boldsymbol{A}) \neq 0$. This condition is automatically satisfied by incorporating the minimum eigenvalue feature detection algorithm[18], which mandates that the eigenvalues of $\boldsymbol{A}^{\mathrm{T}}\boldsymbol{A}$ for a feature point are greater than a user-defined threshold. In practice, interrogation windows containing features comprising bright pixels can be used for tracking. The solution to Eq. (3) is obtained via an iteration scheme proposed in Ref.[15].

Tracking motion in dual-channel fluorescence images

With our experimental setup, we record image pairs from both the beads and the FluoroCubes before and after removal of the adherent cell, producing two pairs of images that share the same displacement field. We test different approaches to track the displacements of the beads and FluoroCubes based on points detected independently from each channel. First, displacements in both channels are tracked individually using the conventional KLT algorithm, and the tracking results are combined to obtain a dense displacement field. Second, dual-channel images can be converted to single-channel images by weighted summation of the intensities. A simple choice is to assign the same weight to both channels and average the images as

$$I(x,y) = 0.5\, I^{(1)}(x,y) + 0.5\, I^{(2)}(x,y), \tag{7}$$

where the superscripts indicate the image channel. The resulting averaged image can used for motion tracking with the conventional KLT algorithm. Third, as an alternative approach for extracting information from two images channel, we modify the original KLT algorithm by extending the dimensions of the matrix A given in Eq. (2) as

$$\begin{pmatrix} I_x(x_1,y_1) & I_y(x_1,y_1) \\ \cdots & \\ I_x(x_n,y_n) & I_y(x_n,y_n) \end{pmatrix} \rightarrow \begin{pmatrix} I_x^{(1)}(x_1,y_1) & I_y^{(1)}(x_1,y_1) \\ \cdots & \\ I_x^{(1)}(x_n,y_n) & I_y^{(1)}(x_n,y_n) \\ I_x^{(2)}(x_1,y_1) & I_y^{(2)}(x_1,y_1) \\ \cdots & \\ I_x^{(2)}(x_n,y_n) & I_y^{(2)}(x_n,y_n) \\ \cdots & \end{pmatrix}, \tag{8}$$

where the superscripts on the matrix entries on the right side indicate the image channels. The KLT algorithm, used with the extended matrix, simultaneously tracks the displacements from both channels while imposing the constraint that the displacement field is the same in both channels. Additionally, this modification avoids cross-channel terms in the target function which result in errors in densely labeled images, as discussed in the Results section. However, if one of the two image channels contains much more noise than the other, e.g., if some fluorescent signals occur in one frame but disappear in the next frame, the precision of the displacements estimated from both channels is degraded by the data from the channel with the larger noise. We prevent this problem by using an iterative tracking routine that imposes for every interrogation window in both channels a different weight that is based on previous tracking results. The choice of weighting factors is in principle flexible. Here, we use for the weighting factor the cross-correlation value associated with every tracked interrogation window with given displacement **u** for the two channels independently as

$$w^c = \frac{\sum_{i=1}^{n}(I^c(\mathbf{x}_i+\mathbf{u},t+1) - \bar{I}^c(\mathbf{x}_i+\mathbf{u},t+1))(I^c(\mathbf{x}_i,t) - \bar{I}^c(\mathbf{x}_i,t))}{\sqrt{\sum_{i=1}^{n}(I^c(\mathbf{x}_i+\mathbf{u},t+1) - \bar{I}^c(\mathbf{x}_i+\mathbf{u},t+1))^2 \sum_{i=1}^{n}(I^c(\mathbf{x}_i,t) - \bar{I}^c(\mathbf{x}_i,t))^2}} \tag{9}$$

where c is the channel index, i is the index denoting the pixels in a local window, and $\bar{I}$ is the mean intensity of the interrogation window. Then, the weighted matrix $\boldsymbol{A}$ becomes

$$\boldsymbol{A} = \begin{pmatrix} w^{(1)} I_x^{(1)}(x_1, y_1) & w^{(1)} I_y^{(1)}(x_1, y_1) \\ \dots \\ w^{(1)} I_x^{(1)}(x_n, y_n) & w^{(1)} I_y^{(1)}(x_n, y_n) \\ w^{(2)} I_x^{(2)}(x_1, y_1) & w^{(2)} I_y^{(2)}(x_1, y_1) \\ \dots \\ w^{(2)} I_x^{(2)}(x_n, y_n) & w^{(2)} I_y^{(2)}(x_n, y_n) \\ \dots \end{pmatrix}. \tag{10}$$

Ideally, a perfectly tracked point should have its maximum cross-correlation value at the center of the cross-correlation matrix in both channels. To use this condition for an assessment of the precision of each track, we define a threshold for the distance between the center of the cross-correlation matrix and the maximum of the cross-correlation values. A tracked point must be re-tracked if either the distance between the center and the maximum exceeds the threshold or if the absolute value of the maximum cross-correlation value is less than a second threshold. We repeat the tracking procedure with updated weights until a predefined termination criterion is reached, i.e., if all tracks are accepted according to above criterium or if a maximum number of iterations is exceeded.

Synthetic TFM images

The performance of the image analysis procedures is assessed with synthetic TFM data. We create 20 elliptical traction patches that are evenly distributed around the periphery of a circular cell with a radius of 8 μm. Each traction patch has a major axis with length 1 μm and a minor axis with length of 0.25 μm, where the major axis point toward the cell center. Traction forces inside each patch point toward the cell center and have a constant magnitude of 500 Pa. Assuming a Young's modulus of 3000.00 Pa and a Poisson's ratio of 0.5, we calculate the exact displacement vectors on a grid with 20 nm spacing. Next, we randomly select a number of grid points as reference positions for fluorescent labels, ensuring a label density of approximately 5 μm^{-2}. A Gaussian point spread function with a standard deviation of 2 pixels is applied to each reference position to generate images. A deformed bead image is acquired similarly, with the new label positions computed based on the previously obtained displacements. We generate two sets of reference-deformed image pairs for two imaging channels. Note that neither background noise nor local variations in PSF are included in the synthetic data for *in silico* assessment of the improvement of the modified optical flow tracking algorithm. Consequently, we only assessed tracking errors resulting from the high density of beads with overlapping point spread functions.

Image preprocessing

Image processing is carried out in MATLAB. The employed functions are written in *italic* below. All raw images of fiducial markers are preprocessed to enhance features, using a difference-of-Gaussian filter with a filter size of 5 pixels in both dimensions. The standard deviations of the Gaussian filters vary depending on the image qualities and are set to 1.5 and 2.5 pixels, respectively. The *imgaussfilt* function is employed for filtering and the *imadjust* is applied for contrast adjustment. Subsequently, marker detection and tracking are done with feature-enhanced images. Before analysis, we correct for a stage shift using *normxcorr2* with subpixel accuracy achieved by fitting the correlation peak with a 2D Gaussian function, implemented with *lsqcurvfit*. After aligning the images, we use *vision.LocalMaximaFinder* or *detectMinEigenFeatures* to determine pixel positions of feature points. For conventional KLT tracking, the posidion of the detected fiducials are then fed into *vision.PointTracker*.

Assessment of image quality and point spread function using fluorescent beads

A customized MATLAB script is used to calculate the signal-to-background ratio and fluorescence intensity profile around every nanobead as shown in Fig. 1. First, the beads are localized using the function *vision.LocalMaximaFinder*. Subsequently, an interrogation window of 7-by-7 pixels is placed on top of every local fluorescence intensity maximum to extract images of the beads. Additionally, images of the background signal are acquired by excluding the extracted bead images through masking. Then, the signal-to-background ratio is computed by averaging the local maximal intensities divided by the average intensity of the background pixels. The average fluorescence intensity profile is computed by averaging the intensities along the horizontal center line for all extracted bead images. For better visualization, the profile is fitted with a Gaussian function. The intensities are normalized by a constant.

References

1. DuFort, C. C., Paszek, M. J. & Weaver, V. M. Balancing forces: architectural control of mechanotransduction. *Nat. Rev. Mol. Cell Biol.* **12**, 308–319 (2011).

2. Polacheck, W. J. & Chen, C. S. Measuring cell-generated forces: a guide to the available tools. *Nat. Methods* **13**, 415–423 (2016).

3. Roca-Cusachs, P., Conte, V. & Trepat, X. Quantifying forces in cell biology. *Nat. Cell Biol.* **19**, 742–751 (2017).

4. Zancla, A., Mozetic, P., Orsini, M., Forte, G. & Rainer, A. A primer to traction force microscopy. *J. Biol. Chem.* **298**, 101867 (2022).

5. Harris, A. K., Wild, P. & Stopak, D. Silicone rubber substrata: a new wrinkle in the study of cell locomotion. *Science* **208**, 177–179 (1980).

6. Dembo, M., Oliver, T., Ishihara, A. & Jacobson, K. Imaging the traction stresses exerted by locomoting cells with the elastic substratum method. *Biophys. J.* **70**, 2008–2022 (1996).

7. Schwarz, U. S. & Soiné, J. R. Traction force microscopy on soft elastic substrates: A guide to recent computational advances. *Biochim. Biophys. Acta BBA-Mol. Cell Res.* **1853**, 3095–3104 (2015).

8. Sabass, B., Gardel, M. L., Waterman, C. M. & Schwarz, U. S. High resolution traction force microscopy based on experimental and computational advances. *Biophys. J.* **94**, 207–220 (2008).

9. Colin-York, H. *et al.* Super-Resolved Traction Force Microscopy (STFM). *Nano Lett.* **16**, 2633–2638 (2016).

10. Stubb, A. *et al.* Fluctuation-based super-resolution traction force microscopy. *Nano Lett.* **20**, 2230–2245 (2020).

11. Xu, Y. *et al.* Super-resolution traction force microscopy with enhanced tracer density enables capturing molecular scale traction. *Biomater. Sci.* **11**, 1056–1065 (2023).

12. Jaqaman, K. *et al.* Robust single-particle tracking in live-cell time-lapse sequences. *Nat. Methods 2008 58* **5**, 695–702 (2008).

13. Willert, C. E. & Gharib, M. Digital particle image velocimetry. *Exp. Fluids* **10**, 181–193 (1991).

14. Holenstein, C. N., Silvan, U. & Snedeker, J. G. High-resolution traction force microscopy on small focal adhesions-improved accuracy through optimal marker distribution and optical flow tracking. *Sci. Rep.* **7**, 41633 (2017).

15. Lucas, B. D. & Kanade, T. An Iterative Image Registration Technique with an Application to Stereo Vision. *Proc. 7th Int. Jt. Conf. Artif. Intell. - Vol. 2* 674–679 (1981).

16. Horn, B. K. P. & Schunck, B. G. Determining optical flow. *Artif. Intell.* **17**, 185–203 (1981).

17. Harris, C. G. & Stephens, M. J. A Combined Corner and Edge Detector. in *Alvey Vision Conference* (1988).

18. Jianbo Shi & Tomasi. Good features to track. in *1994 Proceedings of IEEE Conference on Computer Vision and Pattern Recognition* 593–600 (1994).

19. Balaban, N. Q. *et al.* Force and focal adhesion assembly: a close relationship studied using elastic micropatterned substrates. *Nat. Cell Biol. 2001 35* **3**, 466–472 (2001).

20. Butler, J. P., Tolic-Nørrelykke, I. M., Fabry, B. & Fredberg, J. J. Traction fields, moments, and strain energy that cells exert on their surroundings. *Am. J. Physiol.-Cell Physiol.* **282**, C595–C605 (2002).

21. Huang, Y. *et al.* Traction force microscopy with optimized regularization and automated Bayesian parameter selection for comparing cells. *Sci. Rep.* **9**, 539 (2019).

22. Niekamp, S., Stuurman, N. & Vale, R. D. A 6-nm ultra-photostable DNA FluoroCube for fluorescence imaging. *Nat. Methods* **17**, 437–441 (2020).

23. Axelrod, D. Total Internal Reflection Fluorescence Microscopy in Cell Biology. *Traffic* **2**, 764–774 (2001).

24. Gutierrez, E. *et al.* High refractive index silicone gels for simultaneous total internal reflection fluorescence and traction force microscopy of adherent cells. *PLoS One* **6**, e23807 (2011).

25. Iwadate, Y. & Yumura, S. Molecular dynamics and forces of a motile cell simultaneously visualized by TIRF and force microscopies. *BioTechniques* **44**, 739–750 (2008).

26. Knoll, S. G., Ali, M. Y. & Saif, M. T. A. A Novel Method for Localizing Reporter Fluorescent Beads Near the Cell Culture Surface for Traction Force Microscopy. *J. Vis. Exp.* e51873 (2014).

27. Holmes, D. L. & Stellwagen, N. C. Estimation of polyacrylamide gel pore size from Ferguson plots of linear DNA fragments. II. Comparison of gels with different crosslinker concentrations, added agarose and added linear polyacrylamide. *Electrophoresis* **12**, 612–619 (1991).

28. Damljanovic, V., Christoffer Lagerholm, B. & Jacobson, K. Bulk and micropatterned conjugation of extracellular matrix proteins to characterized polyacrylamide substrates for cell mechanotransduction assays. *BioTechniques* **39**, 847–851 (2005).

29. Subramani, R. *et al.* The Influence of Swelling on Elastic Properties of Polyacrylamide Hydrogels. *Front. Mater.* **7**, (2020).

30. Pierschbacher, M. D. & Ruoslahti, E. Cell attachment activity of fibronectin can be duplicated by small synthetic fragments of the molecule. *Nature* **309**, 30–33 (1984).

31. Hermanson, G. T. Chapter 14 - Microparticles and Nanoparticles. in *Bioconjugate Techniques (Third Edition)* (ed. Hermanson, G. T.) 549–587 (Academic Press, Boston, 2013).

32. van de Linde, S. *et al.* Direct stochastic optical reconstruction microscopy with standard fluorescent probes. *Nat. Protoc.* **6**, 991–1009 (2011).

33. Oakes, P. W., Banerjee, S., Marchetti, M. C. & Gardel, M. L. Geometry Regulates Traction Stresses in Adherent Cells. *Biophys. J.* **107**, 825–833 (2014).

34. Yoshie, H. *et al.* High Throughput Traction Force Microscopy Using PDMS Reveals Dose-Dependent Effects of Transforming Growth Factor-β on the Epithelial-to-Mesenchymal Transition. *J. Vis. Exp.* e59364 (2019).

35. Barbieri, L. *et al.* Two-dimensional TIRF-SIM–traction force microscopy (2D TIRF-SIM-TFM). *Nat. Commun.* **12**, 2169 (2021).

36. Moser, M., Legate, K. R., Zent, R. & Fässler, R. The Tail of Integrins, Talin, and Kindlins. *Science* **324**, 895–899 (2009).

37. Theodosiou, M. *et al.* Kindlin-2 cooperates with talin to activate integrins and induces cell spreading by directly binding paxillin. *eLife* **5**, e10130 (2016).

38. Plotnikov, S. V., Sabass, B., Schwarz, U. S. & Waterman, C. M. High-resolution traction force microscopy. in *Methods in cell biology* vol. 123 367–394 (Elsevier, 2014).

39. Style, R. W. *et al.* Traction force microscopy in physics and biology. *Soft Matter* **10**, 4047–4055 (2014).

40. Sabass, B., Koch, M. D., Liu, G., Stone, H. A. & Shaevitz, J. W. Force generation by groups of migrating bacteria. *Proc. Natl. Acad. Sci.* **114**, 7266–7271 (2017).

41. Duvernoy, M.-C. *et al.* Asymmetric adhesion of rod-shaped bacteria controls microcolony morphogenesis. *Nat. Commun.* **9**, 1120 (2018).

42. Hanke, J., Probst, D., Zemel, A., Schwarz, U. S. & Köster, S. Dynamics of force generation by spreading platelets. *Soft Matter* **14**, 6571–6581 (2018).

43. Banda, O. A., Sabanayagam, C. R. & Slater, J. H. Reference-Free Traction Force Microscopy Platform Fabricated via Two-Photon Laser Scanning Lithography Enables Facile Measurement of Cell-Generated Forces. *ACS Appl. Mater. Interfaces* **11**, 18233–18241 (2019).

44. Ghagre, A. *et al.* Pattern-Based Contractility Screening, a Reference-Free Alternative to Traction Force Microscopy Methodology. *ACS Appl. Mater. Interfaces* **13**, 19726–19735 (2021).

45. Stabley, D. R., Jurchenko, C., Marshall, S. S. & Salaita, K. S. Visualizing mechanical tension across membrane receptors with a fluorescent sensor. *Nat. Methods* **9**, 64–67 (2012).

46. Morimatsu, M., Mekhdjian, A. H., Adhikari, A. S. & Dunn, A. R. Molecular Tension Sensors Report Forces Generated by Single Integrin Molecules in Living Cells. *Nano Lett.* **13**, 3985–3989 (2013).

47. Schlichthaerle, T., Lindner, C. & Jungmann, R. Super-resolved visualization of single DNA-based tension sensors in cell adhesion. *Nat. Commun.* **12**, 2510 (2021).

48. Blakely, B. L. *et al.* A DNA-based molecular probe for optically reporting cellular traction forces. *Nat. Methods* **11**, 1229–1232 (2014).

49. Li, H. *et al.* A reversible shearing DNA probe for visualizing mechanically strong receptors in living cells. *Nat. Cell Biol.* **23**, 642–651 (2021).

50. Rashid, S. A. *et al.* All-Covalent Nuclease-Resistant and Hydrogel-Tethered DNA Hairpin Probes Map pN Cell Traction Forces. *ACS Appl. Mater. Interfaces* **15**, 33362–33372 (2023).

51. Saffioti, N. A., Cavalcanti-Adam, E. A. & Pallarola, D. Biosensors for Studies on Adhesion-Mediated Cellular Responses to Their Microenvironment. *Front. Bioeng. Biotechnol.* **8**, (2020).

52. Kruss, S. *et al.* High-resolution imaging of cellular dopamine efflux using a fluorescent nanosensor array. *Proc. Natl. Acad. Sci.* **114**, 1789–1794 (2017).

53. Auernheimer, J., Dahmen, C., Hersel, U., Bausch, A. & Kessler, H. Photoswitched Cell Adhesion on Surfaces with RGD Peptides. *J. Am. Chem. Soc.* **127**, 16107–16110 (2005).

54. Kadem, L. F. *et al.* Rapid Reversible Photoswitching of Integrin-Mediated Adhesion at the Single-Cell Level. *Adv. Mater.* **28**, 1799–1802 (2016).

55. Huth, S. *et al.* Quantifying force transmission through fibroblasts: changes of traction forces under external shearing. *Eur. Biophys. J.* **51**, 157–169 (2022).